INTERNATIONAL JOURNAL FOR NUMERICAL METHODS IN FLUIDS, VOL. 20, 289–305 (1994)

A NUMERICAL STUDY OF PULSATILE LAMINAR FLOWS IN A PIPE WITH A RING-TYPE CONSTRICTION

Z. D. SHI, T. S. LEE AND S. H. WINOTO

Department of Mechanical and Production Engineering, National University of Singapore, Singapore 0511

SUMMARY

Numerical simulations have been carried out to study pulsatile laminar flows in a pipe with an axisymmetric ring-type constriction. Three types of pulsatile flows were investigated, namely a physiological flow, a pure sinusoidal flow and a non-zero mean velocity sinusoidal flow. The laminar flow governing equations were solved by the SIMPLE algorithm on a non-staggered grid and a modified Crank–Nicolson approximation was used to discretrize the momentum equations with respect to time. The maximum flow Reynolds number (Re) is 100. The Womersley number (N_w) ranges from 0 to 50, with the corresponding Strouhal number (St) ranging from 0 to 3·98. The constriction opening ratio (d/D) and thickness ratio (h/D) are fixed at 0·5 and 0·1 respectively. Within the time period investigated, all these pulsatile flows include both forward and backward flows. The unsteady recirculation region and the recirculation points change in size and location with time. For $N_w \leqslant 1$ and $St \leqslant 1 \cdot 56 \times 10^{-3}$ the three pulsatile flows have the same simple relation between the instantaneous flow rate and pressure loss (Δp) across the constriction and the pressure gradient in the axial direction (dp/dz) in the fully developed flow region. The phase angles between the flow rate and pressure loss and the pressure gradient are equal to zero. With increasing N_w and St, the phase angle between the flow rate and the dp/dz becomes larger and has its maximum value of 90° at $N_w = 50$ and $St = 3 \cdot 98$. The three pulsatile flows also show different relations between the flow rate and the pressure gradient. The pure sinusoidal flow has the largest maximum pressure gradient and the non-zero mean velocity sinusoidal flow has the smallest. For larger N_w and St the fully developed velocity profiles in the fully developed flow region have a smaller velocity gradient along the radial direction in the central region. The maximum recirculation length increases for N_w ranging from 0 to 4·2, while this length becomes very small at $N_w = 50$ and $St = 3 \cdot 98$. The deceleration tends to enlarge the recirculation region and this effect appears for $N_w \geqslant 3$ and $St \geqslant 1 \cdot 43 \times 10^{-2}$. Linear relations exist between the flow rate and the instantaneous maximum values of velocity, vorticity and shear stress.

KEY WORDS pulsatile flow; ring-type constriction; laminar pipe flow

1. INTRODUCTION

In recent years unsteady laminar flows have attracted increasing attention in terms of both numerical studies and experimental investigations owing to their relevance in various engineering and biomedical applications. Unsteady flow has been of interest in the design of pulsatile flow meters.[1] The relation between the flow rate and pressure loss across the constriction can provide a formula for calculating the flow rate from the measured pressure loss. The principle of unsteady laminar flow is also applied to heat transfer devices, since heat transfer can be enhanced by the incipience of flow instability.[2] In the study of intra-cardiac flow and blood vessel stenosis, the pressure loss, the maximum flow velocity,

CCC 0271–2091/95/040289–17

Received February 1994
Revised July 1994

shear stress and recirculation region are parameters of interest because of their relation with the atheroma caused by a large pressure drop across the constriction, the corpuscle damage due to large shear stress and the thrombus phenomena resulting from the recirculation region.[3–6]

In the literature, physiological and sinusoidal flows have often been studied separately.[1–4] In biomedical studies, physiological laminar flows are adopted to investigate blood flow phenomena in which the flow Reynolds number is the order of 10^2.[3,4] *In vitro* studies are often based on a sophisticated and expensive experimental set-up which can realistically simulate physiological flows.[7] In industrial applications such as heat exchangers, pure sinusoidal and non-zero mean velocity sinusoidal flows are used owing to their availability. An investigation is carried out here on both physiological and sinusoidal laminar flows.

The flow in a pipe with a ring-type constriction can be used as a physical model in the study of blood vessel stenosis and intra-cardiac flow, unsteady flow meters and heat exchangers. The objectives of the present work are to investigate the effect of the Womersley number, which is a parameter related to the pulsating frequency, on pulsatile flows in a pipe with a ring-type constriction and to study the effects of flow acceleration and deceleration. The investigation is focused on the pressure loss in the flow passing through the constriction, the pressure gradient along the axial direction in the fully developed flow region, the maximum flow velocity, the maximum vorticity and shear stress, the recirculation length and the flow velocity profiles in the fully developed flow region. The present numerical procedure is applied to calculate the laminar flow in a sudden expansion pipe. The ring-type constriction has an opening of 0·5 and a thickness ratio of 0·1. The maximum flow Reynolds number is 100. The flow Womersley number ranges from 0 to 50, with the corresponding Strouhal number ranging from 0 to 3·98.

2. GOVERNING EQUATIONS AND NUMERICAL PROCEDURE

For the case of unsteady incompressible laminar flow the governing equations are the continuity equation and the Navier–Stokes equations. In an axisymmetric co-ordinate system these equations are given as follows:

continuity equation

$$\frac{\partial}{\partial z}(ru) + \frac{\partial}{\partial r}(rv) = 0, \tag{1}$$

z-direction momentum equation

$$St\frac{\partial u}{\partial t} + \frac{\partial}{\partial z}(u^2) + \frac{1}{r}\frac{\partial}{\partial r}(ruv) = -\frac{\partial p}{\partial z} + \frac{\partial}{\partial z}\left(\frac{2}{Re}\frac{\partial u}{\partial z}\right) + \frac{1}{r}\frac{\partial}{\partial r}\left[\frac{r}{Re}\left(\frac{\partial u}{\partial r} + \frac{\partial v}{\partial z}\right)\right], \tag{2}$$

r-direction momentum equation

$$St\frac{\partial v}{\partial t} + \frac{\partial}{\partial z}(uv) + \frac{1}{r}\frac{\partial}{\partial r}(rv^2) = -\frac{\partial p}{\partial r} + \frac{\partial}{\partial z}\left[\frac{1}{Re}\left(\frac{\partial v}{\partial z} + \frac{\partial u}{\partial r}\right]\right] + \frac{1}{r}\frac{\partial}{\partial r}\left(\frac{2r}{Re}\frac{\partial u}{\partial r}\right) - \frac{1}{Re}\frac{2v}{r^2}. \tag{3}$$

In a general curvature co-ordinate system (ξ, η), equations (1)–(3) can be expressed as

$$\frac{\partial G}{\partial t} + \frac{\partial}{\partial \xi}(E - M) + \frac{\partial}{\partial \eta}(F - N) - S = 0, \tag{4}$$

where

$$\xi = \xi(z, r), \qquad \eta = \eta(z, r). \tag{5}$$

The variables (G, E, M, F, N, S, R) are functions of physical variables (u, v, p) and geometrical variables (z, r):[1,8]

$$G = StJr(0, u, v)^{\mathrm{T}}, \qquad E = Jr(U, uU + P\xi_z, vU + P\xi_r)^{\mathrm{T}}, \qquad F = Jr(V, uV + P\eta_z, vV + P\eta_r)^{\mathrm{T}},$$

$$M = Jr(M_1, M_2, M_3)^{\mathrm{T}}, \qquad N = Jr(N_1, N_2, N_3)^{\mathrm{T}}, \qquad S = Jr(S_1, S_2, S_3)^{\mathrm{T}},$$

$$M_1 = 0, \qquad M_2 = \frac{1}{Re}[(g^{11} + \xi_r^2)u_\xi + (g^{12} + \xi_z\eta_z)u_\eta + \xi_z\xi_r v_\xi + \xi_r\eta_z v_\eta],$$

$$M_3 = \frac{1}{Re}[(g^{11} + \xi_r^2)v_\xi + (g^{12} + \xi_r\eta_r)v_\eta + \xi_z\xi_r u_\xi + \xi_z\eta_r u_\eta],$$

$$N_1 = 0, \qquad N_2 = \frac{1}{Re}[(g^{21} + \xi_\xi\eta_z)u_\xi + (g^{22} + \eta_z^2)u_\eta + \xi_z\eta_r v_\xi + \eta_r\eta_z v_\eta],$$

$$N_3 = \frac{1}{Re}[(g^{21} + \xi_r\eta_r)v_\xi + (g^{22} + \eta_r^2)v_\eta + \xi_r\eta_z u_\xi + \eta_z\eta_r u_\eta],$$

$$S_1 = 0, \qquad S_2 = 0, \qquad S_3 = \frac{p}{r} - \frac{1}{Re}\frac{2v}{r^2}.$$

The curvilinear velocity components U and V and the Cartesian velocity components u and v are related by $U = u\xi_z + v\xi_r$ and $V = u\eta_z + v\eta_r$. The Jacobian J and the contravariant metric tensor components g^{11}, g^{12}, g^{21} and g^{22} are given as

$$J = x_\xi y_\eta - x_\eta y_\xi, \qquad g^{11} = \xi_x^2 + \xi_y^2, \qquad g^{12} = \xi_x\eta_x + \xi_y\eta_y, \qquad g^{21} = g^{12}, \qquad g^{22} = \eta_x^2 + \eta_y^2.$$

The time-dependent term G can be expressed as[3,4]

$$G = \frac{1}{2\pi}\frac{N_w^2}{Re}Jr(0, u, v)^{\mathrm{T}}$$

and the Wormsley number is then considered as the characteristic non-dimensional parameter of unsteady flow.

The non-linear equation (4) is solved by an iterative process in which all the physical variables (u, v, p) are updated as

$$\phi^{n+1} = \phi^n + \delta\phi, \tag{6}$$

where n and $n + 1$ are the previous and current iteration numbers respectively and ϕ represents each of the physical variables. By substituting equation (6) and equation (4), the governing equations can be expressed in incremental form as

$$\frac{\partial \delta G}{\partial t} + \frac{\partial}{\partial \xi}(\delta E - \delta M) + \frac{\partial}{\partial \eta}(\delta F - \delta N) - \delta S = -R. \tag{7a}$$

The residual vector R is calculated by using the values of the variable at level n as

$$R = \frac{\partial G^n}{\partial t} + \frac{\partial}{\partial \xi}(E - M)^n + \frac{\partial}{\partial \eta}(F - N)^n - S^n. \tag{7b}$$

For steady flow the Strouhal number St is zero. Hence the time-dependent terms can be deleted from the equations. Equations (7) are solved by the SIMPLE algorithm[9] on a non-staggered grid. All terms containing the incremental variables (δE, δM, δF, δN, δS) are discretized by three-point difference schemes: hybrid difference schemes are used for convective terms, second-order central schemes for diffusive terms, the first-order forward schemes for pressure terms and backward schemes for the continuity equation. The residual vector is calculated by second-order difference schemes: second-

order upwind schemes are used for convective terms, central schemes for diffusive terms, second-order forward schemes for pressure terms and second-order backward schemes for the continuity equation. At convergence the residual vector is equal to zero and the convergent results have second-order accuracy. For points adjacent to the wall the corresponding second-order difference schemes are also used to ensure the consistency of the scheme accuracy.

A modified Crank–Nicolson scheme is used to discretize the time-dependent terms in the governing equations as

$$\frac{\delta G^{n+1} - \delta G^n}{\Delta t} + \theta X^{n+1} + (1 - \theta) X^n = -R, \tag{8}$$

where

$$X = \frac{\partial}{\partial \xi}(\delta E - \delta M) + \frac{\partial}{\partial \eta}(\delta F - \delta N) - \delta S$$

and θ (= 0–1) is a scheme control parameter: $\theta = 0$ represents the time explicit scheme, $\theta = 1$ the time implicit scheme and $\theta = 0{\cdot}5$ the standard Crank–Nicolson scheme. The optimum θ-value can be determined from numerical tests to obtain non-oscillatory results. In the present work $\theta = 0{\cdot}6$ has been adopted after a series of numerical tests.

Owing to the variation in the main flow direction in pulsatile flows, the discretizations of pressure gradient terms and the continuity equations are adjusted according to the instantaneous main flow direction. The differential terms along the axial direction are approximated by the first-order schemes

$$\frac{\partial \delta \phi}{\partial \xi} = \begin{cases} \dfrac{\delta \phi_{i,j} - \delta \phi_{i-1,j}}{\Delta \xi} + O(\Delta \xi) & \text{for forward flow,} \\ \dfrac{\delta \phi_{i+1,j} - \delta \phi_{i,j}}{\Delta \xi} + O(\Delta \xi) & \text{for backward flow,} \end{cases} \tag{9}$$

and the second-order schemes

$$\frac{\partial \phi}{\partial \xi} = \begin{cases} \dfrac{3\phi i,j - 4\phi_{i-1,j} + \phi_{1-2,j}}{2\Delta \xi} + O(\Delta \xi^2) & \text{for forward flow,} \\ \dfrac{-3\phi_{i,j} + 4\phi_{i+1,j} - \phi_{i+2,j}}{2\Delta \xi} + O(\Delta \xi^2) & \text{for backward flow.} \end{cases} \tag{10}$$

The numerical procedure can then be briefly outlined as follows.

1. At the start of the calculation all variables are set to zero. The fluid in the pipe is considered to be stationary. At each further time step the initial velocity and pressure fields are given by the convergent values of the previous time step and the boundary values of each variable are specified.
2. The momentum equations are solved by sweeping in the positive and the negative r-direction with underrelaxation treatment. The underrelaxation factor is 0·35. The residual of each equation is calculated. Iteration is continued until the residuals of equations reduce to 0·5 of their values at the first iteration.
3. The residual of the continuity equation is calculated and used as the source terms of the pressure correction equation, which is solved by ADI sweeps. The sweep is repeated until the residual of the pressure correction equation reduces to 0·5 of its value at the first iteration.
4. The flow flux at each section in the z-direction is calculated. The maximum equation residual and maximum flux difference from that at the inlet section are obtained. The programme will return to step 2 when the maximum residual or maximum flux difference is greater than 0·01.
5. At convergence the streamline, vorticity and shear stress fields are calculated from the velocity field. Information about the pressure is obtained from the pressure field.

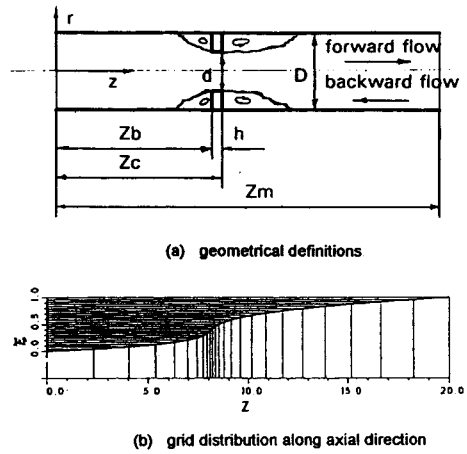

Figure 1. Flow in a pipe with a ring-type constriction: (a) geometrical definitions (Zb = 8.0D, Zc = 8.1D, Zm = 20.0D, h = 0.1D, d = 0.5D); (showing $\frac{1}{5}$ of total grid points); (b) grid distribution along axial direction with more clusters at $z = Z_c$

3. BOUNDARY CONDITIONS

In the solution domain shown in Figure 1(a) the upstream inlet velocity conditions are described as

$$u(r,t) = \frac{(n+1)(2n+1)}{2n^2}\left(1-\frac{2r}{D}\right)^{1/n}\bar{u}(t), \qquad v(r,t) = 0, \tag{11}$$

where $n = 6$ in the present study. This power law rather than a parabolic profile is used, because the velocity profiles of pulsatile flow are generally not parabolic curves. The bulk inlet velocity $\bar{u}(t)$ is specified according to the pulsatile flow as shown in Figure 2.

(i) For the pure sinusoidal flow

$$\bar{u}(t) = \sin\left(2\pi\frac{t}{T_s}\right) = \sin\left(2\pi\frac{t}{T}\frac{13}{8}\right).$$

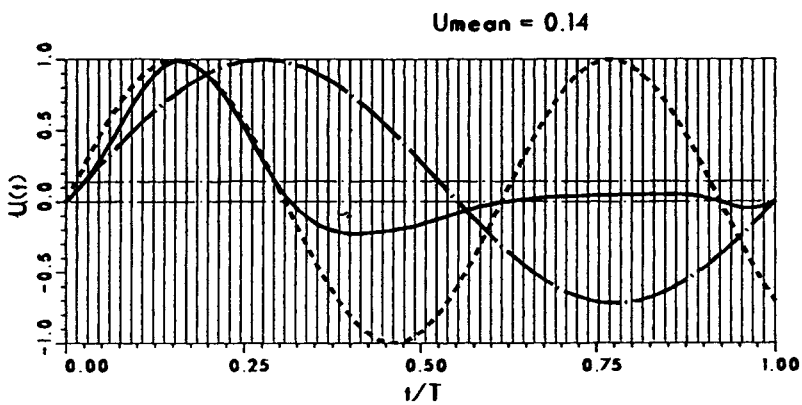

Figure 2. Cross-sectional average velocities of three pulsatile flows: physiological flow (—), sinusoidal flow (– – –) and non-zero mean flow sinusoidal flow (—·—·—)

(ii) For the non-zero mean velocity sinusoidal flow

$$\bar{u}(t) = u_{\text{mean}} + (1 - u_{\text{mean}}) \sin\left(2\pi \frac{t}{T} + \varphi_0\right), \qquad \varphi_0 = -\sin^{-1}\left(\frac{u_{\text{mean}}}{1 - u_{\text{mean}}}\right),$$

with $u_{\text{mean}} = 0{\cdot}14$ the same value as in the physiological flow.

(iii) For the physiological flow $\bar{u}(t)$ is adopted from Reference 10.

At each time step, along the solid wall a no-slip velocity condition is used, i.e. $u = 0$, $v = 0$. Along the central line axisymmetric conditions are applied for all variables, i.e. $\partial u/\partial r = 0, v = 0, \partial p/\partial r = 0$. At the downstream exit section the pressure is fixed to zero and the flow is considered to be fully developed, i.e. $p = 0$, $\partial u/\partial z = 0, \partial v/\partial z = 0$.

4. GRID STRETCHING FUNCTION

In the grid point arrangement within the solution domain a stretching function is used along the axial direction as

$$\frac{\mathrm{d}z}{\mathrm{d}\xi} = z_{\text{m}}[\alpha + \beta(\xi - \xi_1)^2 \gamma^{\xi}], \tag{12}$$

with the boundary conditions

$$z|_{\xi=0} = 0, \qquad z|_{\xi=1} = z_{\text{m}}, \tag{13}$$

where z_{m} is the maximum length of the solution domain in the axial direction and α and γ are two grid control parameters. At point $\xi = \xi_1$ the grid size is $\Delta z = z_{\text{m}}\alpha\Delta\xi$, which can be controlled by the value of α. If $\alpha < 1$, the grid will become more clustered at point $\xi = \xi_1$. The grid distribution for the whole z-region can be further controlled by the parameter γ. After integrating equation (12) and incorporating the boundary conditions, the stretching function can be expressed as

$$\frac{z}{z_{\text{m}}} = \alpha\xi + \beta\frac{\gamma^{\xi}}{\ln\gamma}\left[\xi_1^2 + \frac{2\xi_1}{\ln\gamma} + \frac{2}{\ln^2\gamma} - 2\xi\left(\xi_1 + \frac{1}{\ln\gamma}\right) + \xi^2\right] - \frac{\beta}{\ln\gamma}\left(\xi_1^2 + \frac{2\xi_1}{\ln\gamma} + \frac{2}{\ln^2\gamma}\right), \tag{14}$$

where

$$\beta = \frac{1 - \alpha}{\dfrac{\gamma}{\ln\gamma}\left[\xi_1^2 - 2\xi_1\left(1 - \dfrac{1}{\ln\gamma}\right) + \left(1 - \dfrac{2}{\ln\gamma} + \dfrac{2}{\ln^2\gamma}\right)\right] - \dfrac{1}{\ln\gamma}\left(\xi_1^2 + \dfrac{2\xi_1}{\ln\gamma} + \dfrac{2}{\ln^2\gamma}\right)}.$$

In the present study the grid points are more concentrated near the constriction. The parameter ξ_1 is calculated using the above equation and the constriction location as shown in Figure 1(a). The parameter γ is set to $0{\cdot}2$ according to a grid adjustment test and α is determined from $\Delta z = \Delta r$ in the region near the constriction, i.e. $\alpha = \Delta r/z_{\text{m}}\Delta\xi$. This stretching function is illustrated in Figure 1(b).

5. RESULTS AND DISCUSSION

The numerical procedure was first tested on the steady laminar flow in a sudden expansion pipe with a grid of dimensions 21×61 in the r- and z-directions respectively. The present results are compared with the data of Polland[11] and Napolitano and Cinnella[12] for the recirculation length and wall shear stress in Figure 3.

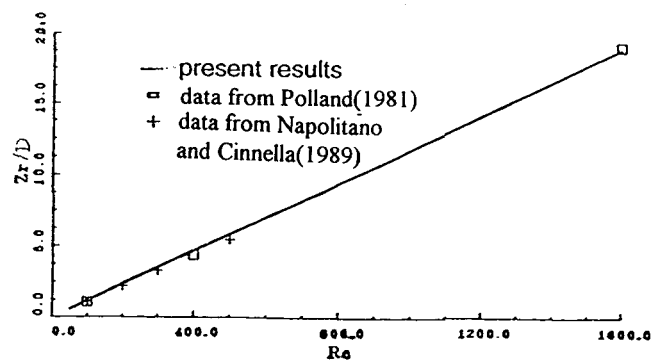

(a) the recirculation lengths

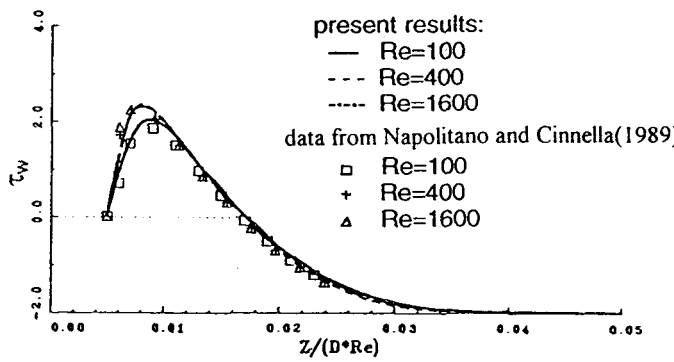

(b) the wall shear stress distribution.

Figure 3. Comparison of results on steady flow in a pipe with a sudden expansion: (a) recirculation length; (b) wall shear stress distribution

In the pulsatile flow simulations the fluid in the pipe is considered to be stationary at the start of the calculation ($t/T = 0$). In order to verify the effect of the initial starting flow condition, the sinusoidal flow in a straight pipe is calculated. As shown in Figure 4, this effect is negligible.

In the calculation of the flow in a pipe with a ring-type constriction the grid points are equally distributed in the radial and time directions. However, in the axial z-direction the grid points are unequally distributed, with more points concentrated near the constriction as shown in Figure 1(b). Grid points totalling 15, 21 and 31 in the r-direction and 81, 101 and 121 in the z-direction are tested under the steady flow conditions. Totals of 31, 41 and 61 grid points in the time direction are tested for the first three time steps to obtain the grid-point-independent numerical results. Further calculations are then based on an arrangement of 21, 121 and 65 grid points in the r-, z- and t-directions respectively.

5.1. The physiological flow fields

In the case of $N_w = 1$ and $St = 1{\cdot}59 \times 10^{-3}$ the physiological flow field development with time is presented in Figure 5. With t/T increasing from 0 to 10/65, the forward flow is accelerated to its peak flow velocity. The recirculation length (z_r/D) increases from zero to a maximum value of 2·74. As t/T

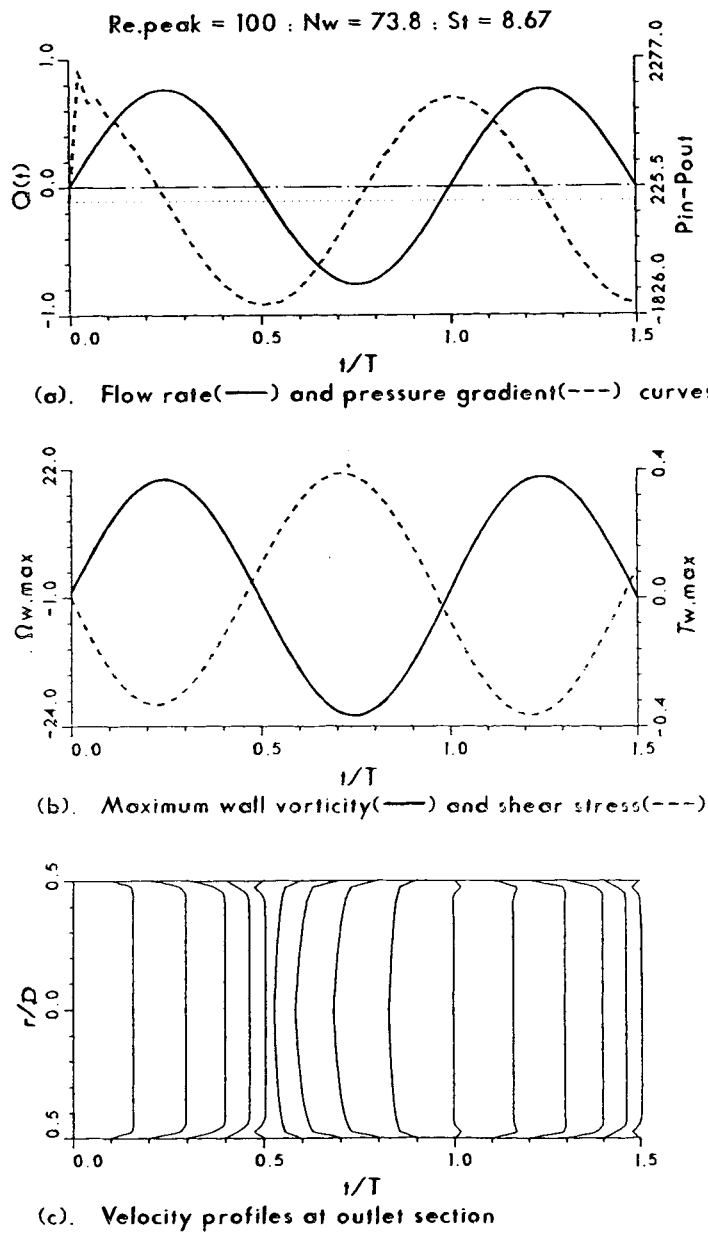

Figure 4. Test on effect of initial starting condition on laminar sinusoidal flow in a straight pipe: (a) pressure difference between inlet and outlet sections; (b) maximum vorticity and shear stress; (c) velocity profiles at downstream outlet section

varies from 10/65 to 20/65, the forward flow is decelerated to zero average flow velocity and z_r/D decreases to zero correspondingly. In the period from $t/T = 20/65$ to 40/65 the main flow is moving backwards. The upstream inlet becomes the downstream outlet and the recirculation region appears on the left side of the constriction. The backward flow has its maximum value of $\bar{u}(t) = -0 \cdot 22$ at $t/T = 26/65$. The recirculation regions are smaller than those of the forward flow because of the lower flow velocity. In the time period from $t/T = 40/65$ to 1 the flow velocity is very low, with $|\bar{u}| < 0 \cdot 06$. The

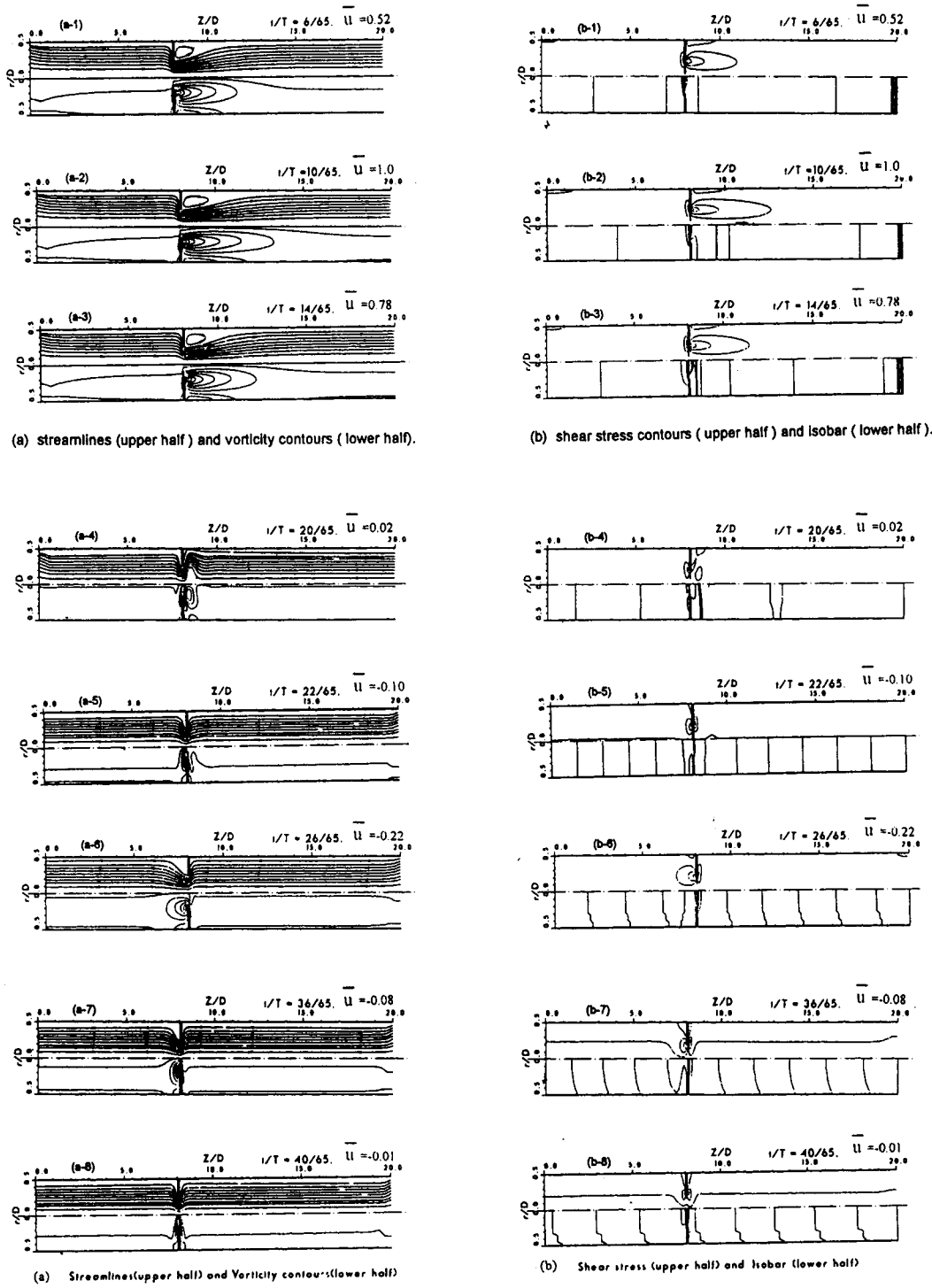

(a) streamlines (upper half) and vorticity contours (lower half).

(b) shear stress contours (upper half) and isobar (lower half).

Figure 5. Physiological flow development in a pipe with a ring-type constriction with $d/D = 0{\cdot}5$ and $h/D = 0{\cdot}1$ in the case of $Re = 100$, $N_w = 1$ and $St = 1{\cdot}59 \times 10^{-3}$: (a) streamlines (upper half) and vorticity contours (lower half); (b) shear stress contours (upper half) and isobars (lower half)

flow fields predicted are similar to those of previous time steps, but with much smaller recirculation regions.

Considering the two cases of $t/T = 20/65$ and $40/65$, the average velocities are nearly equal to zero, corresponding to instantaneous flow Reynolds numbers of 2 and -1 respectively. However, their streamlines and other characteristics contours are quite different. At $t/T = 20/65$ a large vorticity exists in the region on the right side of the constriction. The vorticity cannot diffuse completely within this small time increment, resulting in asymmetric characteristic contours to the constriction. At $t/T = 40/65$ all characteristic contours are nearly symmetrical to the constriction. The instantaneous flow field is nearly a Stokes flow field owing to its very low instantaneous Reynolds number.

Figure 5 shows that there is no constant recirculation region in the physiological flow. The recirculation point moves forwards and backwards with time. In physiological circulation this property is helpful to prevent thrombus phenomena in blood vessels.

5.2. *Effect of Womersley number*

The three types of pulsatile flow are calculated for the Womersley number in the range 0–50, which corresponds to the Strouhal number ranging from 0 to 3·98. The effects of N_w on the flow properties are presented below.

5.2.1. Relation between flow rate (Q) and pressure loss (Δp). The effect of the Womersley number on the relation between the instantaneous flow rate Q and the pressure loss Δp is presented in Figure 6. At $N_w = 1$ the three pulsatile flows have the same relation as at $N_w = 0$, namely

$$\Delta p = 18{\cdot}8Q|Q|, \tag{15}$$

which is plotted as the solid curve in Figure 6. The three pulsatile flows have the same maximum pressure loss at the instant of maximum flow rate. The maximum nondimensional pressure loss is equal to 10·2. This relation is satisfied for all cases of $N_w \leqslant 5$ and $St \leqslant 3{\cdot}98 \times 10^{-2}$ as shown in Figures 6(a)–6(c). However, no simple relation between the flow rate and the pressure loss can be found for higher Womersley numbers, i.e. $N_w \geqslant 10$ and $St \geqslant 0{\cdot}16$, as shown in Figure 6(d).

5.2.2. Relation between flow rate (Q) and pressure gradient (dp/dz). At small Womersley number the instantaneous flow rate Q is linearly related to the instantaneous pressure gradient (dp/dz) along the axial-direction in the fully developed flow region at $z/D = 16$, as shown in Figure 7(a). The phase angle φ_{p-Q}, between the flow rate and the pressure gradient is zero. The pulsatile flow can then be treated as a quasi-steady flow. At $N_w = 1$ the three pulsatile flows have the same relation

$$dp/dz = -0{\cdot}484Q. \tag{16}$$

With increasing Womersley and Strouhal numbers, their relations become elliptic curves, as shown in Figures 7(b)–7(f). The phase angle φ_{p-Q} has its maximum value of 90° at $N_w = 50$ and $St = 3{\cdot}98$. In Figure 7 there are two values of dp/dz corresponding to the same flow rate value at some points for $Q > 0$, because the calculation was carried for slightly more than one complete cycle. The difference between these two values is not small at the first time step where $Q = 0{\cdot}12$. This implies that slightly more than one complete cycle should be calculated in the pulsatile flow simulation. The relations can be expressed as below, where $dp/dz' = (dp/dz)\cos\theta - Q\sin\theta$, $Q' = (dp/dz)\sin\theta + Q\cos\theta$ and θ is the angle between the Q-axis and the elliptic longitudinal axis.

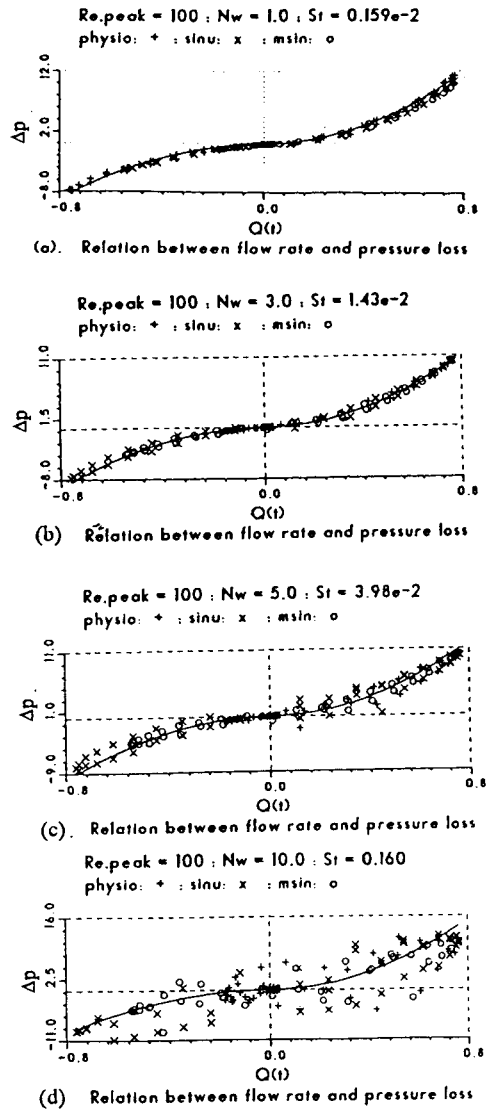

Figure 6. Relation between flow rate and pressure loss for various Womersley numbers

In the case of $N_w = 2$, $St = 0{\cdot}637 \times 10^{-2}$, $\theta = -33°$, $\varphi_{p-Q} = 10°$ and the fitted solid curve as shown in Figure 7(b),

$$\left(\frac{\mathrm{d}p/\mathrm{d}z'}{0{\cdot}071}\right)^2 + \left(\frac{Q'}{0{\cdot}85}\right)^2 = 1 \quad \text{for pure sinusoidal flow} \tag{17}$$

and

$$\left(\frac{\mathrm{d}p/\mathrm{d}z'}{0{\cdot}06}\right)^2 + \left(\frac{Q' - 0{\cdot}136}{0{\cdot}85}\right)^2 = 1 \quad \text{for non-zero mean velocity sinusoidal flow.} \tag{18}$$

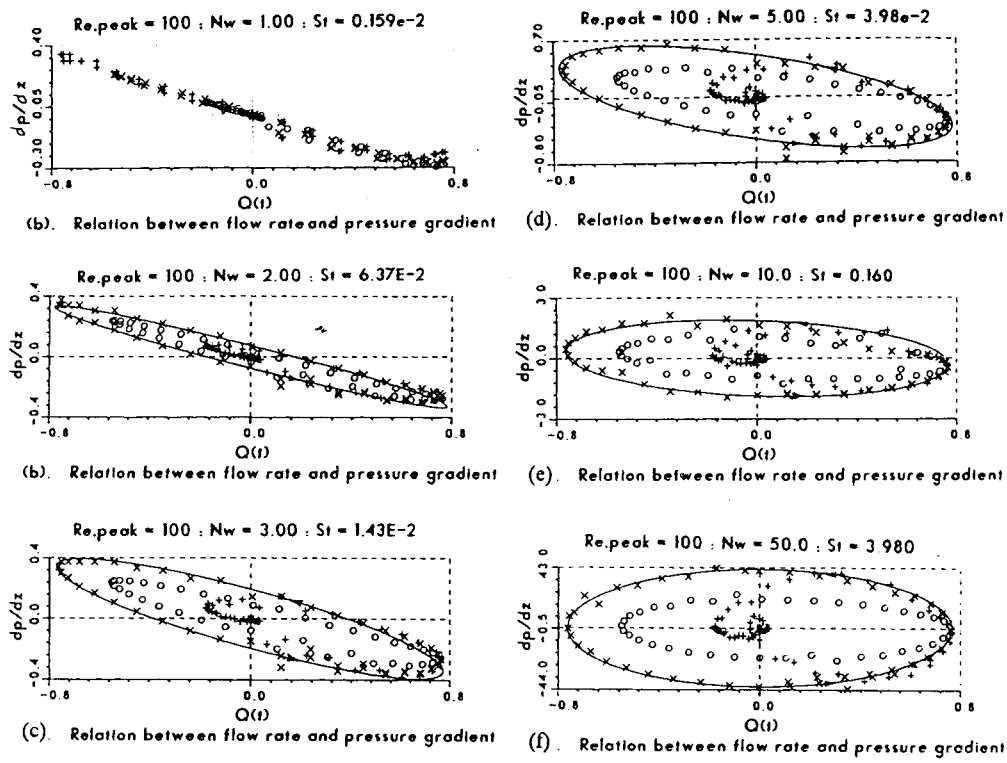

Figure 7. Relation between flow rate and pressure gradient for various Womersley numbers

In the case of $N_w = 3$, $St = 1{\cdot}43 \times 10^{-2}$, $\theta = -23°$, $\varphi_{p-Q} = 30°$ and the fitted solid curve shown in Figure 7(c),

$$\left(\frac{\mathrm{d}p/\mathrm{d}z'}{0{\cdot}181}\right)^2 + \left(\frac{Q'}{0{\cdot}848}\right)^2 = 1 \quad \text{for pure sinusoidal flow} \tag{19}$$

and

$$\left(\frac{\mathrm{d}p/\mathrm{d}z'}{0{\cdot}1}\right)^2 + \left(\frac{Q' - 0{\cdot}13}{0{\cdot}85}\right)^2 = 1 \quad \text{for non-zero mean velocity sinusoidal flow.} \tag{20}$$

In the case of $N_w = 5$, $St = 3{\cdot}98 \times 10^{-2}$, $\theta = -15°$, $\varphi_{p-Q} = 60°$ and the fitted solid curve shown in Figure 7(d),

$$\left(\frac{\mathrm{d}p/\mathrm{d}z'}{0{\cdot}45}\right)^2 + \left(\frac{Q'}{0{\cdot}785}\right)^2 = 1 \quad \text{for pure sinusoidal flow} \tag{21}$$

and

$$\left(\frac{\mathrm{d}p/\mathrm{d}z'}{0{\cdot}35}\right)^2 + \left(\frac{Q' - 0{\cdot}13}{0{\cdot}85}\right)^2 = 1 \quad \text{for non-zero mean velocity sinusoidal flow.} \tag{23}$$

In the case of $N_w = 10$, $St = 0{\cdot}160$, $\theta = -10°$, $\varphi_{p-Q} = 80°$ and the fitted solid curve shown in Figure 7(e),

$$\left(\frac{dp/dz'}{1{\cdot}9}\right)^2 + \left(\frac{Q'}{0{\cdot}785}\right)^2 = 1 \quad \text{for pure sinusoidal flow} \tag{23}$$

and

$$\left(\frac{dp/dz'}{1{\cdot}1}\right)^2 + \left(\frac{Q'}{0{\cdot}785}\right)^2 = 1 \quad \text{for non-zero mean velocity sinusoidal flow.} \tag{24}$$

In the case of $N_w = 50$, $St = 3{\cdot}98$, $\theta = 0°$, $\varphi_{p-Q} = 90°$ and the fitted solid curve shown in Figure 7(f),

$$\left(\frac{dp/dz}{42}\right)^2 + \left(\frac{Q}{0{\cdot}785}\right)^2 = 1 \quad \text{for pure sinusoidal flow} \tag{25}$$

and

$$\left(\frac{dp/dz}{22}\right)^2 + \left(\frac{Q - 0{\cdot}13}{0{\cdot}785}\right)^2 = 1 \quad \text{for non-zero mean velocity sinusoidal flow.} \tag{26}$$

The phase angle φ_{p-Q} is increased to its maximum value of 90°. The maximum pressure gradient appears at the instant of maximum flow acceleration or deceleration, while the instantaneous flow rate is equal to zero.

The effect of the Womersley number on the Q–dp/dz relation becomes important with an increase its value. For small N_w-values such as $N_w < 1$ and $St < 1{\cdot}6 \times 10^{-3}$ the time-dependent terms $St\ \partial(u, v)/\partial t$ are very small and their effect can be neglected. The pulsatile flows can then be treated as quasi-steady flows. The three pulsatile flows have the same maximum pressure loss. At larger N_w- and St-values such as $N_w > 2$ the time-dependent terms become significant for the pressure gradient and differences among the three types of pulsatile flow results appear. The non-zero mean velocity sinusoidal flow has the smallest pressure gradient. The pure sinusoidal flow has roughly the same pressure loss as the physiological flow for larger instantaneous flow rates ($Q > 0{\cdot}2$).

5.2.3. Velocity profiles. The Womersley number has a large effect on the pulsatile flow velocity profiles in the fully developed flow region at $z/D = 16$, as shown in Figure 8 for the sinusoidal flow results. At $N_w = 0$ or 1 and $St = 0$ or $1{\cdot}6 \times 10^{-3}$ the velocity profiles are parabolic. The axial velocity is zero at the instant of zero flow rate, as shown in Figure 8(a) and 8(b). However, for large N_w- and St-values the velocity profiles are no longer parabolic. The velocity gradient along the radial direction becomes small in the central region and large in the region adjacent to the boundary. The axial velocity is not zero at the instant of zero flow rate. At $N_w = 50$ and $St = 3{\cdot}98$ the fluid motion is limited to a small region about $D/10$ from the pipe wall in the complete cycle.

5.2.4. Recirculation length. The sinusoidal flow results are used to investigate the effect of the Womersley number on the recirculation length, as shown in Table I, where $(z_r/D)_{max,1}$ and $(z_r/D)_{max,2}$ are the maximum recirculation lengths in the acceleration and deceleration periods respectively.

During the acceleration period the maximum recirculation length $(z_r D)_{max,1}$, has its largest value at about $N_w = 3$. It becomes zero at $N_w = 50$. However, in the deceleration period the maximum recirculation length $(z_r/D)_{max,2}$, has its largest value at about $N_w = 5$. For $N_w > 3$ the flow deceleration causes a larger recirculation region in the pulsatile flow.

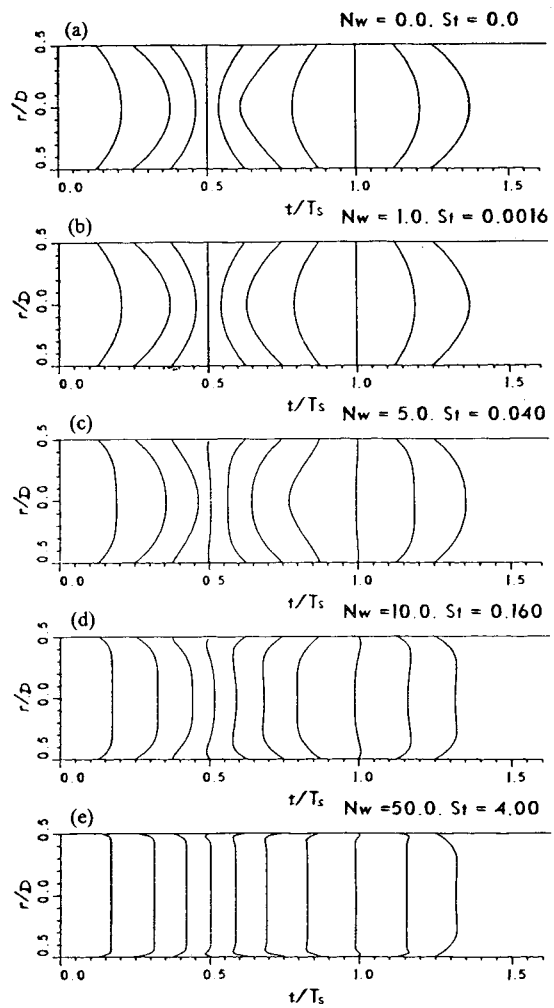

Figure 8. Effect of Womersley and Strouhal numbers on velocity profiles

Table I. Maximum recirculation lengths at various N_w-values

	$N_w = 0$	1	2	3	5	10	30	50
$(z_r/D)_{max,1}$	2·74	2·95	3·10	3·10	2·89	1·36	0·21	0·00
$(z_r/D)_{max,2}$	2·74	2·95	3·10	3·18	4·20	2·92	0·74	0·20

5.2.5. Other parameters of the laminar pulsatile flows. Linear relations exist between the flow rate and the non-dimensional maximum values of flow velocity, vorticity and shear stress as given by

$$u_{max} = 7{\cdot}4Q(t), \qquad 166{\cdot}45Q(t), \qquad \tau_{max} = -1{\cdot}06Q(t) \tag{27}$$

and illustrated in Figure 9 for the case of $N_w = 10$ and $St = 0{\cdot}160$. From these expressions the overall maximum values can be calculated from the flow rate. The wall maximum vorticity and shear stress are about 0·2 of their overall maximum values according to the numerical calculations. In some biofluid

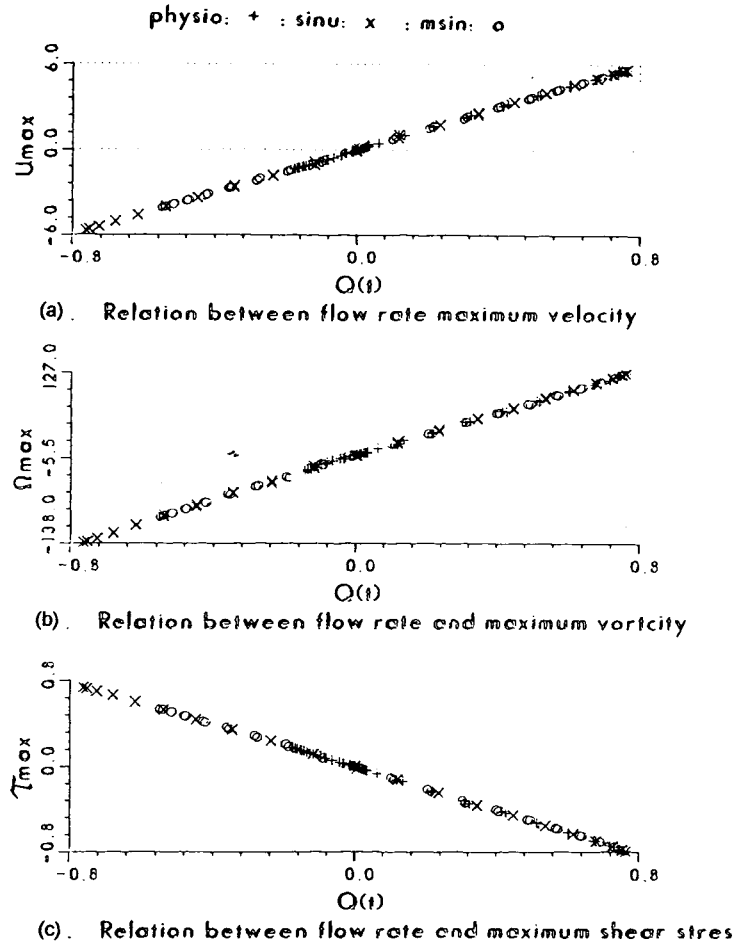

Figure 9. Relations between flow rates and various flow fields parameters: (a) maximum flow velocity; (b) maximum vorticity; (c) maximum shear stress

dynamic investigations, e.g. intracardiac flow and valvular regurgitant flow studies, the velocity information can be obtained from the Doppler echocardiography technique.[13] From the velocity value the maximum shear stress, flow discharge and pressure loss can be estimated through numerical study as in the present work.

5.3. The effect of acceleration and deceleration

As can be seen in Figure 7, acceleration and decelaration have a significant effect on the relation between the flow rate and the pressure gradient for $1 < N_w < 10$ and $1{\cdot}6 \times 10^{-3} < St < 0{\cdot}16$. Acceleration results in a large pressure drop, so more energy is required to transport a unit volume of fluid during acceleration. Their effects on the flow fields are further presented in Figure 10 based on the results of pure sinusoidal flow at $N_w = 5$. At time steps $t/T = 4/65$ and $16/65$ the average velocities are about $0{\cdot}55$ and the acceleration and decelaration have the same value. Figures 10(a) and 10(b) show the differences in the recirculation region, vorticity contours and shear stress contours. Deceleration leads to larger recirculation regions.

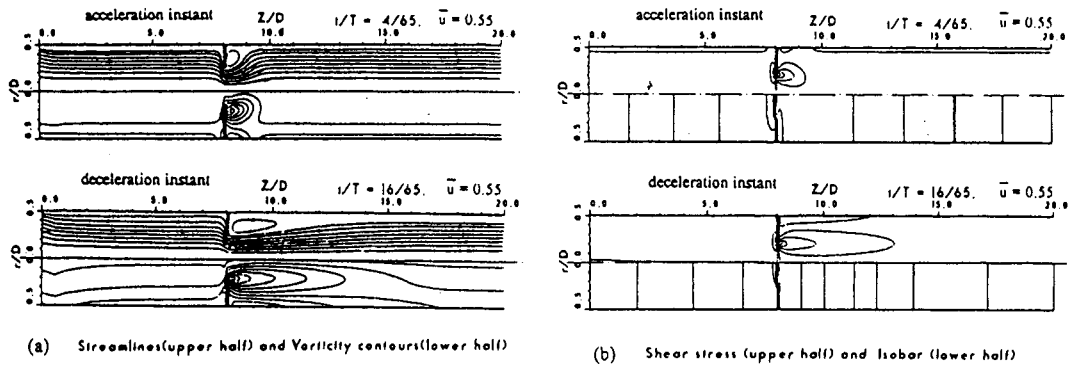

Figure 10. Effect of flow acceleration and deceleration on sinusoidal flow fields in the case of $N_w = 5$ and $St = 4 \times 10^{-2}$: (a) streamlines (upper half) and vorticity contours (lower half); (b) shear stress contours (upper half) and isobars (lower half)

6. CONCLUSIONS

Three types of pulsatile laminar flows in a pipe with a ring-type constriction have been studied. The effect of the Womersley and Strouhal numbers on the flow fields has been investigated in the ranges 0–50 and 0–3·98 respectively. From the numerical results the following conclusions can be drawn.

1. The recirculation region and the recirculation points in the pulsatile flows change in size and location with time owing to the variation in instantaneous flow velocity superimposed on the main flow field. There is no constant flow stationary point in the pulsatile flows.
2. A quadratic relation was found between the instantaneous flow rate and the pressure loss across the constriction for $N_w \leqslant 10$ and $St \leqslant 0{\cdot}160$.
3. With increasing N_w- and St-values, the phase angle between the flow rate and the pressure gradient changes from 0° to 90°. Their relation changes from a linear curve to an elliptic curve for the sinusoidal flows. The maximum pressure gradient over the whole time period becomes larger. The velocity gradient in the radial direction decreases from that of parabolic values to zero in the central region of the pipe. The maximum recirculation region has its peak value at about $N_w = 5$ and $St = 3{\cdot}98 \times 10^{-3}$.
4. For the N_w- and St-values considered, linear relations exist between the flow rate and the maximum values of velocity, vorticity and shear stress.
5. Flow deceleration tends to enlarge the recirculation region and its effect becomes more significant with increasing Womersley and Strouhal numbers, while flow acceleration tends to increase the pressure drop in the pipe flow.
6. With respect to the pressure loss, pressure gradient, overall maximum flow velocity, maximum shear stress and vorticity, the pure sinusoidal flow gives a good approximation to the physiological flow. Hence in biofluid dynamics studies, *in vitro* experiments can be performed using a mechanical sinusoidal flow (with small backward flow) to simulate physiological flow problems.

APPENDIX: NOMENCLATURE

		non-dimensionalized by
D	pipe diameter	L
d	orifice diameter	L

dp/dz	pressure gradient in axial direction	
$\rho U^2 L^{-1} h$	constriction thickness	L
N_w	Womersley number, $N_w = D\sqrt{(\omega/\nu)}$	
p	pressure	ρU^2
Δp	pressure loss in flow passing constriction	ρU^2
Q	flow rate, $Q = Q(t) = (\pi/4)D^2\bar{u}(t)$	UL^2
Q_{max}	non-dimensional maximum flow rate, $\pi/4$	
Re	Reynolds number, $Re = \bar{u}_{peak}D/\nu$	
r	radial co-ordinate, radial distance	L
St	Strouhal number, $St = D/\bar{u}_{peak}T$ or $(1/2\pi)/Nw^2/Re$	
T	time period of physiological flow	T
T_s	time period of physiological flow	T
t	time co-ordinate, time step	T
u	axial velocity component	U
$\bar{u}(t)$	instantaneous bulk velocity in pipe	U
$\bar{u}_{peak}$	peak $\bar{u}(t)$-value	U
v	radial velocity component	U
z	axial co-ordinate, axial distance	L
z_r	recirculation length	L
α_p	underrelaxation factor in updating pressure	
ρ	fluid density	
ξ, η	co-ordinate variables in general curvature co-ordinates	L
ν	fluid molecular kinetic viscosity	
τ	non-dimensional shear stress, $\tau = (1/RE)(\partial u/\partial r + \partial v/\partial z)$	
Ω	non-dimensional vorticity, $\Omega = \partial u/\partial r - \partial v/r\partial z$	
φ_{p-Q}	phase angle between flow rate and pressure loss	

REFERENCES

1. E. H. Jones Jr. and R. A. Bajura, 'A numerical analysis of pulsating laminar flow through a pipe orifice', *ASME J. Fluids Eng.*, **113**, 199–205 (1991).
2. H. Suzuki, Y, Inoue, T. Nishimura, K. Fukutani and K. Suzuki, 'Unsteady flow in a channel obstructed by a square rod (crosscross motion of vortex)', *Int. J. Heat Fluid Flow*, **14**, 2–9 (1993).
3. L. M. Strivastava, 'Flow of couple stress fluid through stenotic blood vessels', *J. Biomech.*, **18**, 479–485 (1985).
4. M. Nakamura and T. Sawada, 'Numerical study on the unsteady flow of non-Newtonian fluid', *ASME J. Biomech. Eng.*, **112**, 100–103 (1990).
5. H. Huang, V. J. Modi, B. R. Seymour and R. Raliga, 'Fluid dynamics of stenosed arteries: a numerical study', *Proc. 6th Int. Conf. on Biomedical Engineering*, 1990, pp. 535–540.
6. Z. Lou and W. J. Yang, 'A computer simulation of the non-Newtonian blood flow at the aortic bifurcation', *J. Biomech.*, **26**, 37–49 (1993).
7. H. W. Sung and A. P. Yoganathan, 'Secondary flow velocity patterns in a pulmonary artery model with varying degrees of valvular pulmonic stenosis: pulsatile in vitro studies', *ASME. J. Biomech. Eng.*, **112**, 88–92 (1990).
8. R. Marcelo, A. Mahamad and C. Ricardo, 'Computation of incompressible turbulent flows by an opposed-differencing scheme', *Numer. Heat Transfer*, **12**, 307–320 (1987).
9. S. V. Patankar, *Numerical Heat Transfer and Fluid Flow*, Hemisphere, Washington, DC, 1980.
10. D. A. McDonald, 'The relation of pulsatile pressure to flow in arteries', *J. Physiol.*, **127**, 533–552 (1955).
11. A. Polland, 'A contribution on the effects of inlet conditions when modelling stenosis using sudden expansions', *J. Biomech.*, **14**, 349–355 (1981).
12. M. Napolitano and P. Cinnella, 'A numerical study of planar and axially-symmetric sudden expansion flows', *Comput. Fluids*, **17**, 185–193 (1989).
13. A. S. Pearlman and C. M. Otto, 'Quantification of valvular regurgitation: a review of cardiovascular ultrasound', *Echocardiography*, **4**, 271–287 (1987).
14. D. A. Steinman, Bach Vinh, C. R. Ethier, M. Ojha, R. S. C. Cobbold and K. W. Johnston, qoA numerical simulation of flow in a two-dimensional end-to-side anastomosis model', *ASME J. Biomed. Eng.*, **115**, 112–118 (1993).
15. W. Y. Soh and J. W. Goodrich, 'Unsteady solution of incompressible Navier–Stokes equations', *J. Comput. Phys.* **79**, 113–134.